Article

Discovery Medicine 2025; 37(201): 2428–2438
https://doi.org/10.24976/Discov.Med.202537201.205

Targeting Inflammatory and Fibrotic Responses: Butorphanol Orchestrates Wound Healing by Suppressing the IL-6/p38/JNK Pathway

Minlie Yang[1], Yang Yang[1], Gaofeng Shi[1], Yun Guo[1], Tianfan Xuan[1], Dan Sun[1], Lingtao Ding[1,*], Xian Ding[2,*]

[1]Burns and Trauma Treatment Center, Affiliated Hospital of Jiangnan University, 214122 Wuxi, Jiangsu, China
[2]Department of Anesthesiology, Affiliated Hospital of Jiangnan University, 214122 Wuxi, Jiangsu, China
*Correspondence: dinglingt00@126.com (Lingtao Ding); dingxian_dx36@163.com (Xian Ding)
Submitted: 13 June 2025 Revised: 28 August 2025 Accepted: 4 September 2025 Published: 20 October 2025

Background: Excessive inflammation and fibrosis during wound healing can cause delayed repair and pathological scar formation. This study aimed to investigate the effects of butorphanol on inflammation and fibrosis during wound healing and to explore the underlying molecular mechanisms.

Methods: A rat burn wound model was established and treated with varying doses of butorphanol. Wound closure rates were recorded on days 3, 7, 10, and 14 post-injury. Histological analyses were performed to assess tissue repair and fibrosis. Expression levels of pro-inflammatory cytokines, macrophage polarization markers, fibrosis-related proteins, and p38/c-Jun N-terminal kinase (JNK) signaling molecules were measured using real-time quantitative polymerase chain reaction (RT-qPCR), immunohistochemistry, and Western blotting. Pharmacological inhibitors and agonists targeting the interleukin-6 (IL-6)/p38/JNK pathway were applied to validate mechanistic involvement.

Results: Butorphanol significantly accelerated wound healing, reduced inflammatory cell infiltration, and downregulated pro-inflammatory cytokines in the early stages ($p < 0.05$). It promoted macrophage polarization toward the anti-inflammatory M2 phenotype by increasing Cluster of Differentiation (CD)206 expression and suppressing CD86 expression ($p < 0.05$). Temporally, butorphanol enhanced the early expression of fibrosis-associated markers to support the transition to the proliferative phase, while suppressing their excessive late-stage expression to prevent pathological scarring ($p < 0.05$). Mechanistically, butorphanol inhibited activation of the IL-6/p38/JNK signaling pathway, as evidenced by altered pathway activity following pharmacological modulation, thereby regulating inflammation and fibrosis during healing ($p < 0.05$).

Conclusion: Butorphanol promotes orderly wound healing by modulating inflammation and fibrosis through regulation of the IL-6/p38/JNK signaling axis. These findings establish butorphanol as a promising therapeutic candidate for enhancing burn wound repair, and offer new perspectives on the IL-6/p38/JNK axis as a potential molecular target for regulating inflammation and fibrosis.

Keywords: butorphanol; wound healing; inflammation; macrophage polarization; fibrosis

Introduction

Wound healing is a dynamic, tightly regulated biological process through which the body restores tissue integrity and function following skin or tissue injury [1]. This process typically progresses through three overlapping phases: inflammation, proliferation, and remodeling. While most wounds heal effectively under normal physiological conditions, the process is often accompanied by the formation of scar tissue [2]. Scars are fibrotic tissues resulting from aberrant collagen overproduction and disorganized deposition during dermal reconstruction, reflecting the incomplete restoration of the original tissue architecture and function [3]. The primary contributors to scar formation include excessive early inflammation, abnormal fibroblast activation, imbalanced collagen synthesis, and dysregulation of signaling pathways regulating extracellular matrix (ECM) remodeling [4,5]. Pathological scars, including hypertrophic scars and keloids, commonly arise in the context of deep burns, extensive trauma, or impaired healing environments [6]. Current therapeutic approaches, such as pharmacological agents, physical therapies, and surgical excision, are limited by suboptimal efficacy, high recurrence rates, and adverse side effects [7]. Beyond cosmetic concerns, scar formation may cause pruritus, pain, and functional impairment, imposing significant psychological and financial burdens on patients [8]. Therefore, elucidating the mechanisms of scar formation during wound healing and developing safer, more effective interventions remain central goals in regenerative medicine and tissue repair research.

Butorphanol is a synthetic opioid analgesic that acts as a κ-opioid receptor agonist and partial μ-opioid receptor agonist [9]. It provides strong analgesic efficacy, favorable safety, and minimal respiratory depression, making it widely used for postoperative, obstetric, and cancer-related pain management. Recent studies suggest that butorphanol may also facilitate wound healing. In Sprague-Dawley (SD) rat models, butorphanol significantly accelerated wound healing, reduced pro-inflammatory cytokines interleukin-1 (IL-1) and interleukin-6 (IL-6), and increased anti-inflammatory interleukin-10 (IL-10) expression by day 10 post-operation, thereby shortening healing time and improving wound repair [10]. Interleukin-6 (IL-6) is a pleiotropic type II cytokine essential for immune regulation, cell proliferation, and tissue repair [11]. IL-6 activates downstream mitogen-activated protein kinase (MAPK) and phosphoinositide 3-kinase (PI3K) signaling cascades to regulate cell proliferation, migration, and differentiation [12]. Previous research has demonstrated that butorphanol suppresses the proliferation and metastasis of hepatocellular carcinoma cells by modulating MAPK signaling, particularly by inhibiting phosphorylation of p38 and c-Jun N-terminal kinase (JNK) [13]. Both p38 and JNK phosphorylation play key roles in wound healing. The p38 kinase cascade is essential for wound contraction, while JNK inhibition promotes the differentiation and migration of epidermal keratinocytes, thereby accelerating wound repair [14]. Therefore, the present study aimed to investigate the potential mechanisms underlying the effects of butorphanol on wound healing, focusing on its potential to attenuate excessive inflammation and fibrotic scar formation by inducing macrophage polarization toward an anti-inflammatory phenotype. Moreover, we explored the involvement of the IL-6/p38/JNK signaling pathway in mediating these effects. A deeper understanding of butorphanol's role in modulating inflammatory responses and fibrosis may not only reveal novel mechanisms of scar mitigation but also support its therapeutic potential as a multifunctional agent to improve wound healing outcomes.

Materials and Methods

Animals

A total of 72 SD rats (8–10 weeks old; approximately 300 g) were obtained from Hangzhou Medical College (Hangzhou, China). Rats were housed under controlled conditions (22 ± 2 °C, 55 ± 10% humidity, 12-hour light/dark cycle) with free access to water and standard chow. Animals were acclimatized for one week before experimentation.

Animal Grouping

SD rats were randomly divided into four groups (n = 12 per group): Control, Butorphanol-Low (B-L), Butorphanol-Medium (B-M), and Butorphanol-High (B-H). A burn wound model was established as previously described [15]. Briefly, rats were anesthetized with 4% isoflurane (R510-22-10, RWD, Shenzhen, China). After shaving the dorsal hair, depilatory cream (PH1877, Phygene, Fuzhou, China) was administered for three minutes. A pre-heated 8 mm diameter metal rod (xk-materials, Changsha, China), immersed in hot water, was applied to the raised dorsal skin for 10 seconds to induce a standardized burn. Following injury, rats in the B-L, B-M, and B-H groups received subcutaneous butorphanol injections (027-19003, FUJIFILM Wako, Guangzhou, China) at doses of 1 mg/kg, 2.5 mg/kg, and 5 mg/kg, respectively, four times daily for 14 days [13]. Control rats received equal volumes of normal saline (ST341, Beyotime, Shanghai, China) on the same interval. All animals were hydrated and treated with topical ketoprofen gel (https://www.bjhanmi.com.cn/front/en/cpzx_3_2.jsp, Hanmi Pharmaceutical, Beijing, China) for analgesia before being returned to individual cages.

On days 3, 7, 10, and 14 post-injury, burn sites were photographed under 4% isoflurane anesthesia using a stereomicroscope fitted with an Amscope MD200 camera (AmScope, Los Angeles, CA, USA). Relative wound area (%) was calculated as wound area/original wound area × 100%. No abnormalities in animal activity, feeding, drinking, or hair condition were observed during the study. On days 3, 7, 10, and 14, three animals from each group were anesthetized with isoflurane (3% induction, 1.5% maintenance) mixed with compressed air, and euthanized by intravenously-administered pentobarbital (150 mg/kg, P3761, Sigma-Aldrich, St Louis, MO, USA). Burn tissues were excised, bisected, and utilized for gene expression tests on one half and histological analysis on the other.

In a separate experiment, SD rats were randomly divided into four groups (n = 6 per group): Control, B-H, B-H + Exogenous IL-6 (FIL-6), and B-H + Anisomycin. FIL-6 was prepared by pre-mixing recombinant interleukin-6 (IL-6, 500 ng, 506-RL, R&D Systems, Shanghai, China) with recombinant soluble IL-6 receptor alpha subunit (sIL-6Rα, 500 ng, HEK293, MCE, Shanghai, China) in a 1:1 molar ratio. One hour after burn induction, rats in the B-H, B-H + FIL-6, and B-H + Anisomycin groups received 5 mg/kg of butorphanol subcutaneously four times daily for 14 days. Additionally, the B-H + FIL-6 group received intravenous FIL-6 once daily for 14 days [16], while the B-H + Anisomycin group received intravenous injection of the JNK activator anisomycin (5 mg/kg, HY-18982, MCE, Shanghai, China) once daily for 14 days [17]. Control group treatment and analgesia were as described above. No abnormalities in animal behavior, feeding, drinking, or hair condition were observed. On days 3 and 14, three animals per group were anesthetized under isoflurane anesthesia, and euthanized by intravenously-administered pentobarbital (150 mg/kg, P3761, Sigma-Aldrich, St Louis, MO, USA), and burn tissues were collected, bisected, and used for histology and expression analysis.

Table 1. Primers used for real-time PCR in this study.

Gene	Forward Primer (5′-3′)	Reverse Primer (5′-3′)
IL-6	TCTTGGTCCTTAGCCACTCC	TCTTGGTCCTTAGCCACTCC
IL-1β	CTATGTCTTGCCCGTGGAG	CTGCTTGAGAGGTGCTGATG
TNF-α	TCTTCTCATTCCTGCTCGTG	GAGGCTGACTTTCTCCTGGT
COL3α1	CAAGGCTGCAAGATGGATGC	AGCTGAACTGAAAGCCACCA
COL1α1	GGTGGTTATGACTTCAGCTTCC	CAGTACTCTCCGCTCTTCCAGT
GAPDH	CCGGGAAACTGTGGCGTGATGG	AGGTGGAGGAGTGGGTGTCGCTGTT

PCR, polymerase chain reaction; *IL-6*, interleukin-6; *IL-1β*, interleukin-1 beta; *TNF-α*, tumor necrosis factor-alpha; *COL3α1*, collagen type III alpha 1; *COL1α1*, collagen type I alpha 1; *GAPDH*, glyceraldehyde-3-phosphate dehydrogenase.

Histological Analysis

Burn tissues were fixed, embedded in paraffin (8002-74-2, Nanjing Reagent, Nanjing, China), and sectioned at 5 μm thickness. Consecutive sections from different time points were mounted on slides. Hematoxylin and eosin (HE) staining (C0105, Beyotime, China) was performed to evaluate wound structure and area. Masson's trichrome staining (C0189, Beyotime, China) was used to assess collagen and muscle fiber deposition in various sections. Stained tissues were examined under a light microscope (200×; Nikon Eclipse 80i, Nikon, Tokyo, Japan). Positively stained muscle and collagen were quantified using ImageJ software (1.47v, National Institutes of Health, Bethesda, MD, USA).

Reverse Transcription Quantitative Polymerase Chain Reaction (RT-qPCR)

Total RNA was extracted from burn tissues using TRIzol reagent (A33250, Thermo Fisher Scientific, Waltham, CA, USA). RNA was reverse-transcribed into complementary DNA (cDNA) using a reverse transcription kit (04379012001, Roche, Basel, Switzerland). Quantitative PCR was performed on an ABI PRISM 7300 Real-Time PCR system (Applied Biosystems, Waltham, CA, USA) with SYBR Green PCR Master Mix (4344463, Thermo Fisher Scientific, Waltham, CA, USA). Primer sequences (Tsingke, Beijing, China) are listed in Table 1. Glyceraldehyde-3-phosphate dehydrogenase (*GAPDH*) served as the internal reference. Relative gene expression was calculated using the $2^{-\Delta\Delta CT}$ method. For group comparisons, the expression ratio of each target gene to *GAPDH* in the Control group was normalized to 100%, and the ratios of the experimental groups were expressed relative to this baseline.

Immunohistochemistry (IHC)

Paraffin-embedded burn tissue sections (5 μm) were subjected to antigen retrieval in citrate buffer (C2488, Sigma-Aldrich, St Louis, MO, USA). Following washing, sections were blocked with 5% bovine serum albumin (BSA, ST025, Beyotime, China) for one hour. Primary antibodies against CD86 (ab238468, Abcam, Cambridge, UK), CD206 (18704-1-AP, Proteintech, Wuhan, China), and alpha-smooth muscle actin (α-SMA, AF1032, Affbiotech, Liyang, China) were applied and incubated overnight at 4 °C. Following PBS (C0221A, Beyotime, Shanghai, China) washes, sections were incubated for one hour with HRP-conjugated goat anti-rabbit IgG H&L (ab205718, Abcam, Cambridge, UK) or goat anti-mouse IgG H&L (ab150119, Abcam, Cambridge, UK) secondary antibodies. Staining was visualized using a 3,3′-diaminobenzidine (DAB) substrate kit (ab64238, Abcam, Cambridge, UK), and counterstained with hematoxylin (H9627, Sigma-Aldrich, St Louis, MO, USA). Images were captured under a light microscope (400×, Nikon Eclipse 80i, Nikon, Tokyo, Japan), and positive staining (brown) was quantified with ImageJ software (1.47v, National Institutes of Health, Bethesda, MD, USA).

Western Blotting (WB)

Burn tissues were lysed in radioimmunoprecipitation assay (RIPA) buffer (P0013, Beyotime, Shanghai, China). Protein concentrations were determined, and equal amounts of protein were separated by 10% sodium dodecyl sulfate-polyacrylamide gel electrophoresis (SDS-PAGE, P0690, Beyotime, Shanghai, China). Proteins were transferred onto polyvinylidene fluoride (PVDF) membranes (FFP24, Beyotime, Shanghai, China). Membranes were blocked with 5% non-fat milk, incubated overnight at 4 °C with primary antibodies (Table 2), washed, and then probed with HRP-conjugated secondary antibodies for one hour. Bands were visualized using a chemiluminescence detection kit (KGC4902, KeyGene, Nanjing, China) and imaged with the ChemiDoc™ XRS system (Bio-Rad, Hercules, CA, USA). Band intensities were quantified using ImageJ software (1.47v, National Institutes of Health, Bethesda, MD, USA). Relative protein expression was calculated as the target protein gray value/GAPDH gray value. For group comparisons, the Control group ratio was normalized to 100%, and experimental groups were expressed relative to this baseline.

Table 2. Antibodies used in western blot analysis.

Antibody name	Molecular weight	Host	Dilution	Catalog number	Supplier	Type
p-p38	43 kDa	Rabbit	1:1000	#9211	CST	Primary antibody
p38	40 kDa	Rabbit	1:1000	#9212	CST	Primary antibody
p-JNK	46, 54 kDa	Rabbit	1:1000	#9251	CST	Primary antibody
JNK	46, 54 kDa	Rabbit	1:1000	#9252	CST	Primary antibody
GAPDH	36 kDa	Rabbit	1:1000	ab201822	Abcam	Primary antibody
Goat Anti-Rabbit IgG H&L (HRP)		Goat	1/2000	ab6721	Abcam	Secondary antibody

p-p38, phosphorylated p38; p-JNK, phosphorylated JNK; JNK, c-Jun N-terminal kinase.

Statistical Analysis

GraphPad Prism v8.0 (GraphPad, San Diego, CA, USA) was used for data analysis, with the results expressed as mean ± standard deviation (SD). The Shapiro-Wilk test and Levene's test were employed to assess data normality and variance homogeneity, respectively. Repeated-measures analysis of variance (ANOVA) was applied to Fig. 1B for comparisons among multiple groups. Two-way ANOVA was performed for Figs. 2,3 and Fig. 1D–F, while one-way ANOVA was employed for all other comparisons. Post hoc multiple comparisons were performed using Tukey's test, Sidak's test (Fig. 1D–F and Figs. 2,3), or Dunnett's test (Fig. 1B). **Supplementary Table 1** presents the results of normality and equal variance tests for the data. A p-value < 0.05 was considered statistically significant.

Results

Butorphanol Suppresses Excessive Inflammation and Promotes Wound Healing in Rats

On day 7, the wound area of the high-dose butorphanol group (B-H) was significantly lower than that of the Control group (Fig. 1A,B, $p < 0.01$). The wound areas in the B-L and B-M group showed no significant difference compared to the Control group (Fig. 1A,B, $p > 0.05$). By days 10 and 14, the wound area of the B-L, B-M, and B-H groups was considerably reduced relative to the Control group, with wound size decreasing in a dose-dependent manner (Fig. 1A,B, $p < 0.05$). Accordingly, the B-H group was chosen for further investigation.

Histological analysis revealed that on day 3, the Control group exhibited marked inflammatory cell infiltration and capillary dilation. In contrast, the B-H group exhibited significantly reduced inflammatory cell infiltration compared to the Control group, accompanied by evident neovascularization and fibroblast activation (Fig. 1C). From days 7 to 14, the B-H group consistently exhibited fewer inflammatory cells and a faster resolution of inflammation compared to the Control group. Conversely, the Control group maintained persistent and pronounced inflammatory cell infiltration (Fig. 1C).

Although the B-H group initially promoted fibroblast activation, the number of fibroblasts gradually declined with prolonged treatment, reaching levels lower than in the Control group on days 10 and 14 (Fig. 1C). These findings suggest that B-H treatment effectively controls early inflammatory responses, accelerates inflammation resolution, and regulates the repair process by preventing excessive fibroblast accumulation (Fig. 1C). Additionally, on days 3, 7, and 10, levels of pro-inflammatory cytokines such as interleukin-6 (*IL-6*), interleukin-1 beta (*IL-1*β), and tumor necrosis factor-alpha (*TNF-*α) were significantly reduced in the B-H group compared to the Control group (Fig. 1D–F, $p < 0.01$). By day 14, no significant differences were observed between the groups (Fig. 1D–F). IHC demonstrated that on days 3, 7, 10, and 14, CD206 expression was significantly higher, whereas CD86 expression was lower, in the B-H group relative to the Control group (Fig. 2A–C, $p < 0.05$).

Butorphanol Alleviates Fibrotic Scar Formation

On day 3, the expression of alpha-smooth muscle actin (α-SMA) in the B-H group was significantly higher than in the Control group (Fig. 2D,E, $p < 0.01$). However, on days 10 and 14, α-SMA levels in the B-H group were markedly lower than those in the Control group (Fig. 2D,E, $p < 0.05$). On days 3 and 7, the expression of collagen type III alpha 1 (*COL3*α*1*) and collagen type I alpha 1 (*COL1*α*1*) was significantly upregulated in the B-H group relative to the Control group (Fig. 3A,B, $p < 0.01$). By days 10 and 14, however, levels of both indicators in the B-H group were noticeably reduced (Fig. 3A,B, $p < 0.01$). Masson's trichrome staining further revealed that on day 14, collagen content in the B-H group was significantly lower than in the Control group (Fig. 3C,D, $p < 0.01$).

Butorphanol Modulates IL-6/p38/JNK Signaling to Suppress Inflammation and Attenuate Fibrotic Scar Formation

The B-H group exhibited markedly lower ratios of phosphorylated-p38 (p-p38)/p38 and p-JNK/JNK on days 3, 7, and 10 compared to the Control group (Fig. 3E–G, $p < 0.01$). By day 14, no significant differences were observed between groups (Fig. 3E–G). On day 3, levels of *IL-6*, *IL-1*β, *TNF-*α, and CD86 were significantly reduced in the B-H group, whereas CD206 expression was elevated relative to the Control group (Fig. 4A–G, $p < 0.05$). In contrast, the B-H + FIL-6 and B-H + Anisomycin groups

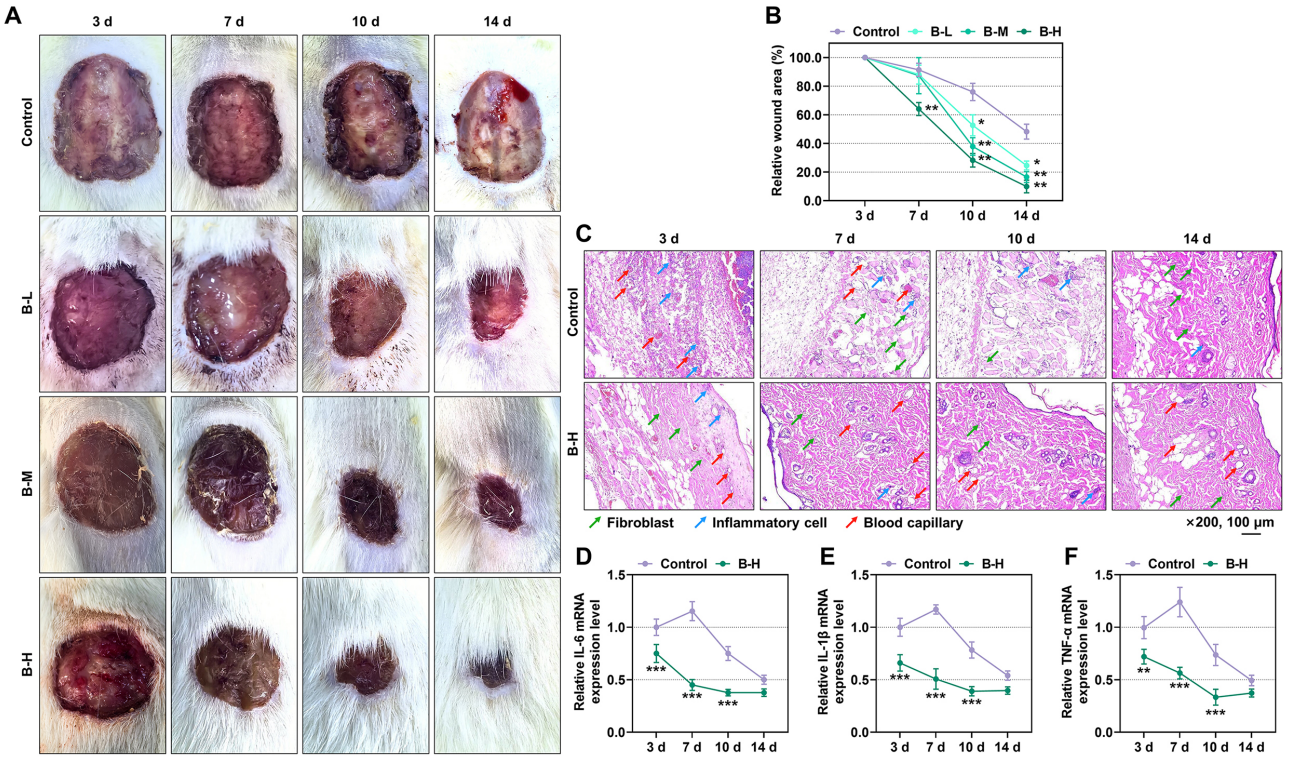

Fig. 1. Butorphanol modulates wound healing and inflammatory cytokine expression. (A,B) Relative wound area on days 3, 7, 10, and 14 in the Control, Butorphanol-Low (B-L), Butorphanol-Medium (B-M), and Butorphanol-High (B-H) groups were determined using the graph paper tracing method. (C) Hematoxylin and eosin (HE) staining of burn wound tissues from Control and B-H groups on days 3, 7, 10, and 14. Magnification: 200×; scale bar: 100 μm. Green arrow: Fibroblast; Blue arrow: Inflammatory cell; Red arrow: Blood capillary. (D–F) Relative mRNA expression levels of interleukin-6 (*IL-6*), interleukin-1 beta (*IL-1β*), and tumor necrosis factor-alpha (*TNF-α*) in burn tissues from Control and B-H groups on days 3, 7, 10, and 14, measured by reverse transcription quantitative polymerase chain reaction (RT-qPCR). Glyceraldehyde-3-phosphate dehydrogenase (*GAPDH*) served as the internal reference. Three rats were randomly selected at each time point; n = 12 rats per group. $^{*}p < 0.05$, $^{**}p < 0.01$, $^{***}p < 0.001$ vs. Control.

showed markedly higher *IL-6*, *IL-1β*, *TNF-α*, and CD86 levels, along with reduced CD206 expression, compared to the B-H group (Fig. 4A–G, $p < 0.01$). On day 14, the expression of *COL3α1*, *COL1α1*, and α-SMA was significantly lower in the B-H group than in the Control group (Fig. 4H,I and Fig. 5A,B, $p < 0.001$). Conversely, the B-H + FIL-6 and B-H + Anisomycin groups exhibited significantly higher levels of these fibrosis markers compared to the B-H group (Fig. 4H,I and Fig. 5A,B, $p < 0.05$). HE staining of burn tissues on day 14 showed normal fibroblast numbers in the Control group, but more pronounced inflammatory cell infiltration than in the B-H group (Fig. 5D). The B-H group demonstrated significantly reduced fibroblast numbers with minimal inflammatory infiltration, whereas the B-H + FIL-6 and B-H + Anisomycin groups exhibited the opposite pattern (Fig. 5D). Furthermore, on day 14, the collagen levels in the B-H group were significantly lower than in the Control group ($p < 0.01$, Fig. 5C,E). In contrast, the B-H + FIL-6 and B-H + Anisomycin groups showed a pronounced increase in collagen content compared to the B-H group ($p < 0.05$, Fig. 5C,E).

Discussion

Inflammation control represents a critical phase in the wound healing process [18]. While moderate and timely inflammation facilitates the clearance of pathogens and necrotic tissue and initiates regenerative mechanisms, excessive or prolonged inflammatory responses can cause additional tissue injury and delayed wound closure [19]. For example, chronic inflammation constitutes a major barrier to wound healing in diabetic models [20]. In severe burns, persistently elevated inflammatory cytokines are strongly associated with hypertrophic scar formation [21]. In the present study, we observed that *IL-6*, *IL-1β*, and *TNF-α* expression peaked on day 7 post-injury, whereas butorphanol treatment significantly downregulated these pro-inflammatory mediators and reduced immune cell infiltration in burn tissue, indicating strong anti-inflammatory potential. A previous study reported that butorphanol promotes wound healing in SD rats by markedly downregulating IL-1 and IL-6, upregulating the anti-inflammatory cytokine IL-10 on day 10, and accelerating wound closure [10]. Our findings are consistent with these observa-

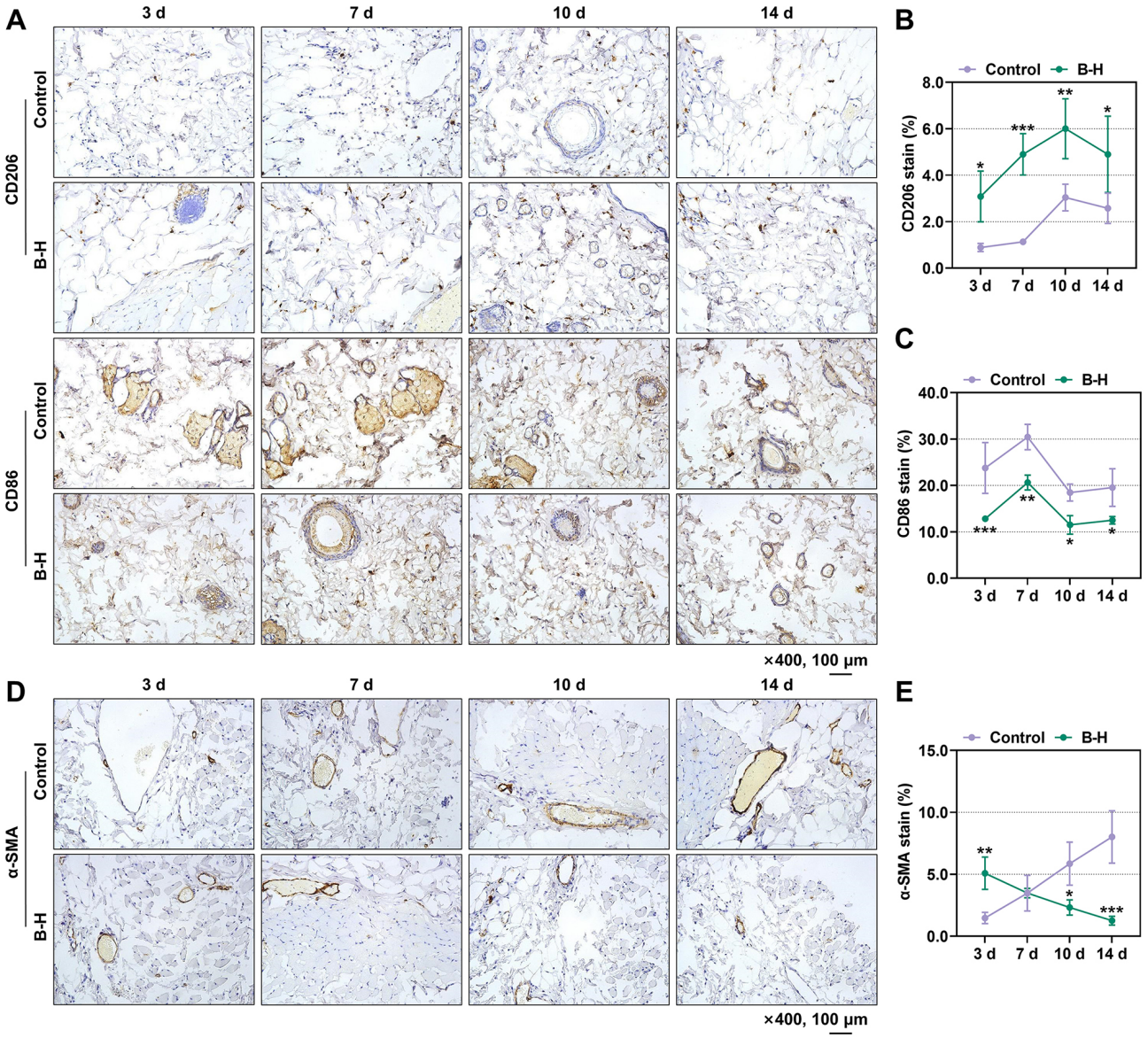

Fig. 2. Butorphanol regulates macrophage polarization and alpha-smooth muscle actin (α-SMA) expression. (A–C) Immunohistochemical staining of CD206 and CD86 in burn tissues from Control and B-H groups on days 3, 7, 10, and 14. Magnification: 400×; scale bar: 100 μm. (D,E) Immunohistochemical staining of α-SMA in burn tissues from Control and B-H groups on days 3, 7, 10, and 14. Magnification: 400×; scale bar: 100 μm. Three rats were randomly selected at each time point; n = 12 rats per group. $^{*}p < 0.05$, $^{**}p < 0.01$, $^{***}p < 0.001$ vs. Control.

tions, further supporting the pro-healing effects of butorphanol. Additionally, in a full-thickness burn model using Dgka$^{-/-}$ mice, enhanced macrophage infiltration was associated with significantly reduced wound area, underscoring the regulatory role of macrophages in wound healing [15]. Similarly, in our study, butorphanol upregulated the M2 macrophage marker CD206 and suppressed the M1 marker CD86 during the early healing phase, suggesting that it promotes a phenotypic shift toward anti-inflammatory macrophage polarization. As macrophages are pivotal regulators of inflammation and repair, their subtype balance directly influences cytokine release and tissue regeneration [22]. Collectively, our findings indicate that butorphanol facilitates wound healing in the early phase by promoting M2 macrophage polarization and suppressing excessive inflammation, thereby downregulating pro-inflammatory cytokines.

Moreover, we observed that butorphanol transiently upregulated α-SMA, *COL3α1*, and *COL1α1* expression during the early wound healing stage, while significantly inhibiting their sustained elevation in later phases. α-SMA serves as a marker of myofibroblast activation, whereas COL3α1 and COL1α1 encode key structural components of collagen involved in scar formation [23,24]. These find-

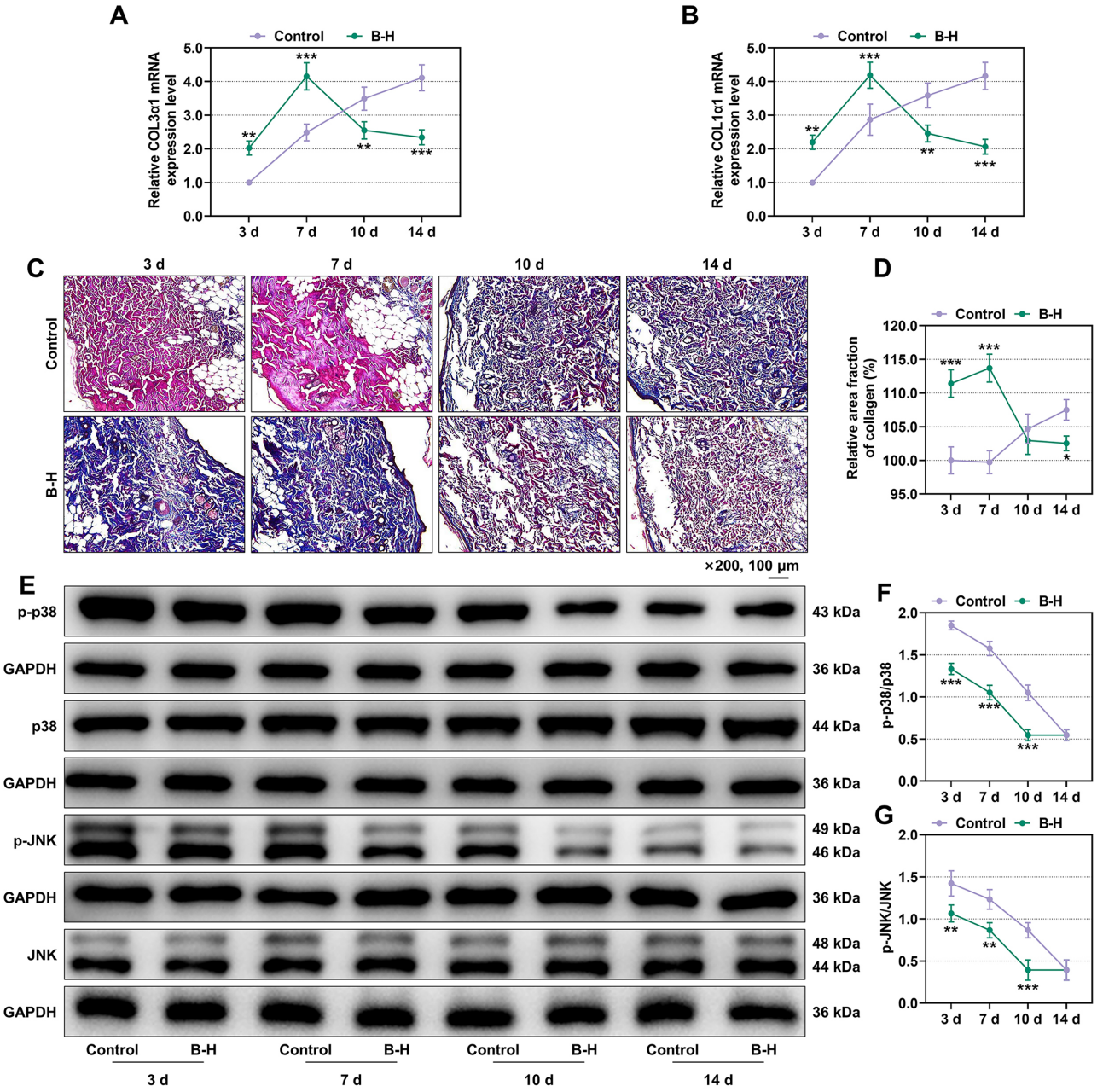

Fig. 3. Butorphanol regulates fibrotic scar formation through the IL-6/p38/c-Jun N-terminal kinase (JNK) signaling pathway. (A,B) RT-qPCR analysis of collagen type III alpha 1 chain (*COL3α1*) and collagen type I alpha 1 chain (*COL1α1*) expression in burn tissues from Control and B-H groups on days 3, 7, 10, and 14. *GAPDH* served as the internal reference. (C,D) Masson's trichrome staining of scar tissues from the Control and B-H groups on days 3, 7, 10, and 14. (E–G) Western blot analysis of phosphorylated p38 (p-p38), p38, phosphorylated JNK (p-JNK), and JNK levels in burn tissues from Control and B-H groups on days 3, 7, 10, and 14. GAPDH served as the internal reference. Magnification: 200×; scale bar: 100 μm. Three rats were randomly selected at each time point; n = 12 rats per group. $^{*}p < 0.05$, $^{**}p < 0.01$, $^{***}p < 0.001$ vs. Control.

ings suggest that butorphanol exerts stage-specific regulatory effects during wound repair. In the early inflammatory phase, infiltration of immune cells activates fibroblasts and induces collagen deposition [25,26]. Butorphanol may attenuate excessive infiltration while supporting fibroblast activation and matrix production, thereby promoting the transition from inflammation to the proliferative phase. At later stages, butorphanol inhibits excessive collagen accumulation, thereby reducing the risk of hypertrophic scarring. This biphasic regulation may represent a mechanism through which butorphanol balances wound healing efficiency with scar quality. Notably, butorphanol also downregulated α-SMA expression during the early stage and subsequently upregulated collagen levels at later time

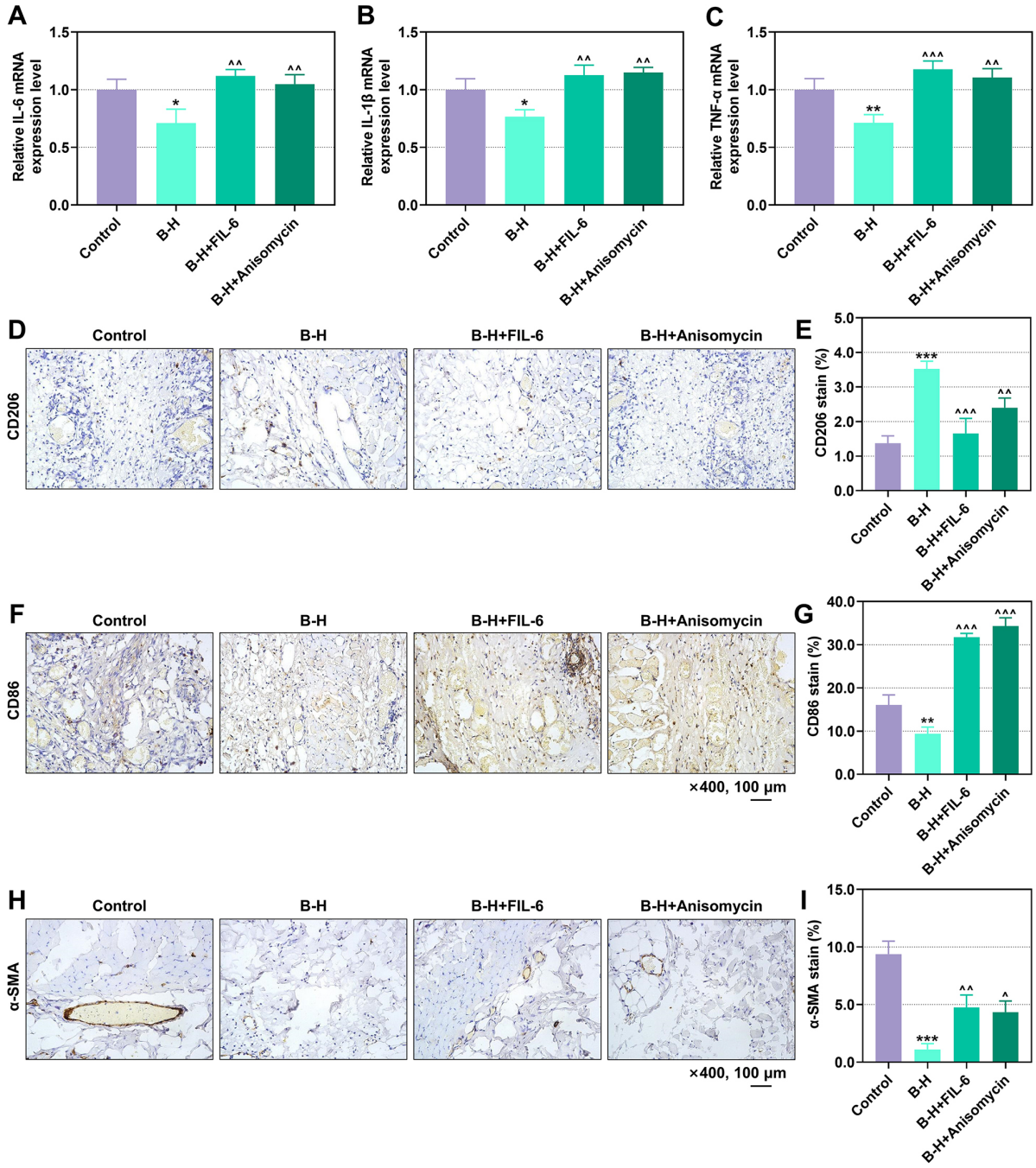

Fig. 4. Butorphanol modulates inflammatory cytokine expression and macrophage polarization via the IL-6/p38/JNK pathway. (A–C) RT-qPCR analysis of *IL-6*, *IL-1β*, and *TNF-α* expression in burn tissues from Control, B-H, B-H + Exogenous IL-6 (FIL-6), and B-H + Anisomycin groups on day 3. *GAPDH* served as the internal reference. (D–G) Immunohistochemical staining of CD206 and CD86 in burn tissues from the four groups on day 3. Magnification: 400×; scale bar: 100 μm. (H,I) Immunohistochemical staining of α-SMA in burn tissues from the four groups on day 14. Magnification: 400×; scale bar: 100 μm. Three rats were randomly selected at each time point; n = 6 rats per group. $^{*}p < 0.05$, $^{**}p < 0.01$, $^{***}p < 0.001$ vs. Control; $^{\wedge}p < 0.05$, $^{\wedge\wedge}p < 0.01$, $^{\wedge\wedge\wedge}p < 0.001$ vs. B-H.

points, suggesting a dynamic role in fibrosis regulation. Collectively, these findings suggest that butorphanol mitigates abnormal scar formation and facilitates tissue remodeling by temporally regulating the expression of fibrosis-associated biomarkers.

Given the central role of inflammation in wound healing, we hypothesize that the late-stage antifibrotic effects of butorphanol may be mediated through modulation of the inflammation-fibrosis axis. Our mechanistic investigations support this hypothesis. Butorphanol significantly in-

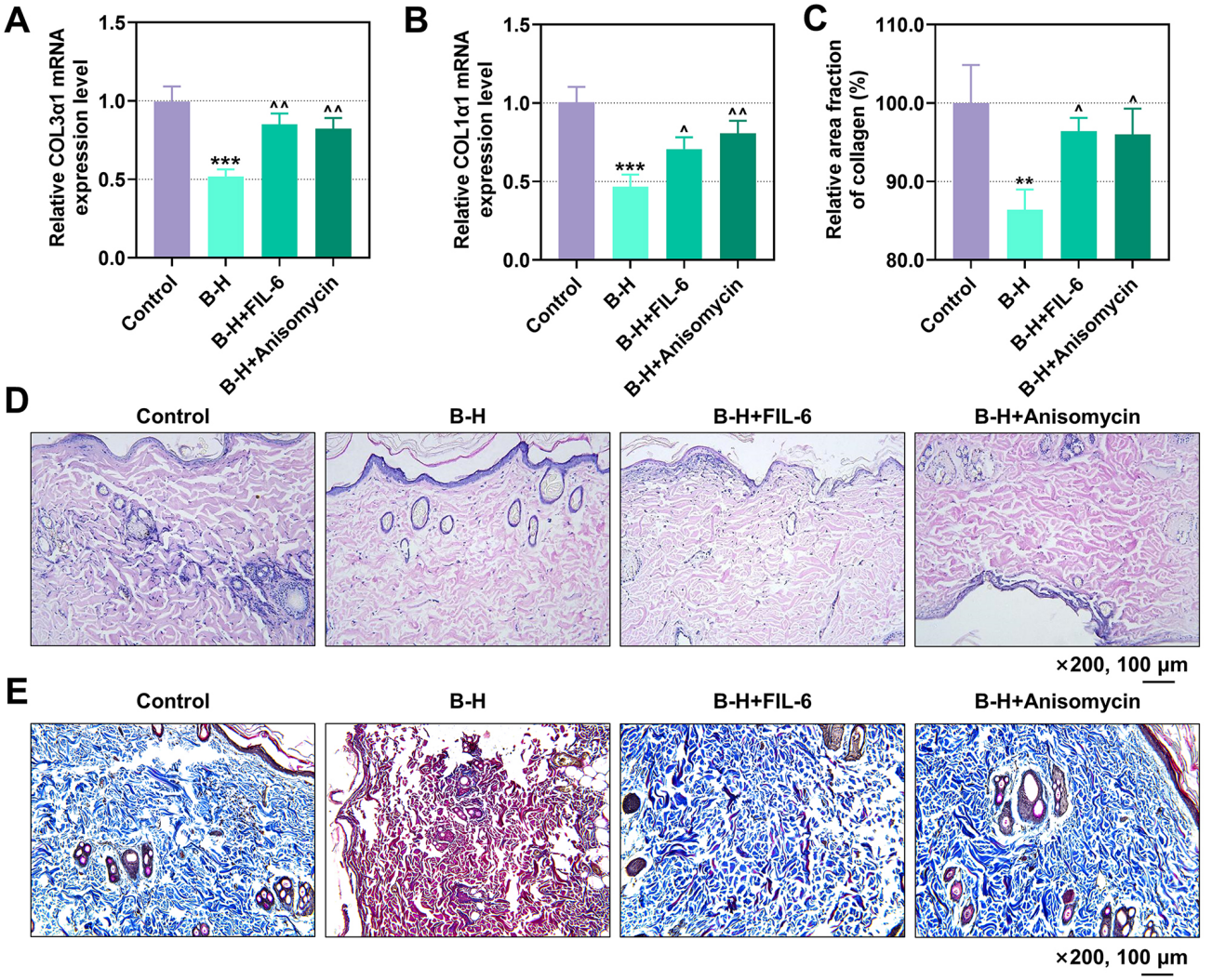

Fig. 5. Butorphanol attenuates fibrotic scar formation via the IL-6/p38/JNK signaling pathway. (A,B) RT-qPCR analysis of *COL3α1* and *COL1α1* expression in burn tissues from Control, B-H, B-H + FIL-6, and B-H + Anisomycin groups on day 14. *GAPDH* served as the internal reference. (D) HE staining of burn tissues from the four groups on day 14. Magnification: 200×; scale bar: 100 μm. (C,E) Masson's trichrome staining of burn tissues from the four groups on day 14. Magnification: 200×; scale bar: 100 μm. Three rats were randomly selected at each time point; n = 6 rats per group. $^{**}p < 0.01$, $^{***}p < 0.001$ vs. Control; $^{\wedge}p < 0.05$, $^{\wedge\wedge}p < 0.01$ vs. B-H.

hibited phosphorylation of p38 and JNK, key downstream components of the IL-6 signaling cascade [12]. Previous studies have emphasized the significance of the p38/JNK pathways in scar formation [27,28]. Wang *et al.* [29] reported that bone morphogenetic protein 1 (BMP1) promotes fibroblast proliferation, migration, and ECM deposition in keloids by activating the p38 signaling pathway. Qin *et al.* [30] demonstrated that staphylococcal nuclease and tudor domain containing 1 (SND1) facilitate keloid formation by activating telomerase through the JNK signaling pathway. Additionally, Liu *et al.* [31] observed that tumor necrosis factor-stimulated gene-6 (TSG-6), secreted by human umbilical cord-derived mesenchymal stem cells (MSCs), alleviates burn-induced excessive inflammation by suppressing p38 and JNK activity. Moreover, previous work showed that butorphanol reduces neuronal inflammatory responses and apoptosis by inhibiting the p38/JNK/ATF2/p53 signaling axis [32]. Consistently, our results indicate that butorphanol suppresses the IL-6/p38/JNK pathway, thereby modulating both early inflammatory responses and downstream fibrotic remodeling, reinforcing its biphasic regulatory role in wound repair. Furthermore, studies in mice have shown a mechanotransduction pathway activated by mechanical force and mediated by focal adhesion kinase (FAK)-extracellular signal-related kinase (ERK)-monocyte chemoattractant protein-1 (MCP1/CCL2) signaling, leading to inflammation-driven fibrosis [33]. Notably, other studies have demonstrated that butorphanol decreases MCP1 expression [34,35]. These findings suggest that butorphanol may act synergistically through multiple targets and pathways. Additional experiments are needed to further validate this possibility.

Despite these promising findings, several limitations must be acknowledged. First, this study was performed using a rat burn wound model, which may not fully capture the complexity of human wound healing and scar formation. Future research will utilize diabetic wound models, porcine skin models, and humanized systems (e.g., 3D skin cultures) to validate the universality of the regulation of inflammation and fibrosis by butorphanol through the IL-6/p38/JNK pathway in more complex wounds and across species. Additionally, this study did not systematically evaluate the systemic toxicity risks of long-term butorphanol treatment (e.g., its effects on the immune system, nervous system, and organ function), nor did it explore the clinical risk-benefit balance, limiting the translational applicability of the findings. Further investigations will evaluate the impact of age, comorbidities (e.g., diabetes) and genetic background on the efficacy of butorphanol, thereby enhancing translational potential. Finally, although pharmacological inhibitors were used to confirm the involvement of IL-6 and p38/JNK pathways, genetic approaches such as gene knockdown or overexpression are needed to provide deeper mechanistic insights.

Conclusion

This study demonstrated that butorphanol, a κ-opioid receptor agonist, effectively enhances wound healing while suppressing excessive inflammation and fibrotic scarring in a rat burn model. These effects are achieved through the downregulation of pro-inflammatory cytokines, upregulation of the M2 macrophage marker CD206, and suppression of fibrosis-associated markers in a time-dependent manner. Mechanistically, butorphanol exerts these actions by inhibiting the IL-6/p38/JNK signaling pathway, as further validated by pathway-specific agonists. Collectively, these findings highlight butorphanol as a promising therapeutic candidate for improving wound healing outcomes in burn injuries and provide novel insights into the IL-6/p38/JNK axis as a potential molecular target for regulating inflammation and fibrosis.

Availability of Data and Materials

The datasets used and/or analyzed during the current study are available from the corresponding authors upon reasonable request.

Author Contributions

MY and YY designed the research study; MY, GS, YG and TX performed the research; YG, DS, LD and XD collected and analyzed the data. MY, YY and GS have been involved in drafting the manuscript and all authors have been involved in revising it critically for important intellectual content. All authors give final approval of the version to be published. All authors have participated sufficiently in the work to take public responsibility for appropriate portions of the content and agreed to be accountable for all aspects of the work in ensuring that questions related to its accuracy or integrity.

Ethics Approval and Consent to Participate

All animal experiments were approved by the Institutional Animal Care and Use Committee (IACUC) of Zhejiang Provincial Laboratory Animal Center (ZJCLA) and conducted in compliance with the institutional guidelines for the laboratory animal care and use (Approval No.: ZJCLA-IACUC-20011039).

Acknowledgment

Not applicable.

Funding

This work was supported by the Top Talent Support Program for young and middle-aged people of Wuxi Health Committee [grant number BJ2023053].

Conflict of Interest

The authors declare no conflict of interest.

Supplementary Material

Supplementary material associated with this article can be found, in the online version, at https://doi.org/10.24976/Discov.Med.202537201.205.

References

[1] Mamun AA, Shao C, Geng P, Wang S, Xiao J. Recent advances in molecular mechanisms of skin wound healing and its treatments. Frontiers in Immunology. 2024; 15: 1395479. https://doi.org/10.3389/fimmu.2024.1395479.

[2] Peña OA, Martin P. Cellular and molecular mechanisms of skin wound healing. Nature Reviews. Molecular Cell Biology. 2024; 25: 599–616. https://doi.org/10.1038/s41580-024-00715-1.

[3] Sullivan JV, Myers S. 1 - Skin structure and function, wound healing and scarring. Plastic Surgery-Principles and Practice (pp. 1–14). Elsevier: Amsterdam. 2022. https://doi.org/10.1016/B978-0-323-65381-7.00001-0.

[4] Ma Y, Liu Z, Miao L, Jiang X, Ruan H, Xuan R, *et al*. Mechanisms underlying pathological scarring by fibroblasts during wound healing. International Wound Journal. 2023; 20: 2190–2206. https://doi.org/10.1111/iwj.14097.

[5] Hong YK, Chang YH, Lin YC, Chen B, Guevara BEK, Hsu CK. Inflammation in Wound Healing and Pathological Scarring. Advances in Wound Care. 2023; 12: 288–300. https://doi.org/10.1089/wound.2021.0161.

[6] Toia F, Rosatti F, Cordova A. Wound healing: physiology and pathology. Textbook of Plastic and Reconstructive Surgery: Basic Principles and New Perspectives (pp. 15–25). Springer International Publishing: Cham. 2022.

[7] Fernández-Guarino M, Bacci S, Pérez González LA, Bermejo-Martínez M, Cecilia-Matilla A, Hernández-Bule ML. The Role

of Physical Therapies in Wound Healing and Assisted Scarring. International Journal of Molecular Sciences. 2023; 24: 7487. https://doi.org/10.3390/ijms24087487.

[8] desJardins-Park HE, Gurtner GC, Wan DC, Longaker MT. From Chronic Wounds to Scarring: The Growing Health Care Burden of Under- and Over-Healing Wounds. Advances in Wound Care. 2022; 11: 496–510. https://doi.org/10.1089/wound.2021.0039.

[9] Hou X, Qu L, Xu Y, Liu J, Guo J. Anti-tumor activity of butorphanol in colorectal cancer via targeting SIGMAR1. Discover Oncology. 2024; 15: 711. https://doi.org/10.1007/s12672-024-01581-1.

[10] Yan L, Lin L, Pushu Z, Junjiang L. Study on the Effects and Mechanism of Butorphanol Combined with Ropivacaine Analgesia on Wound Healing and Scar Formation in Rats. Chinese Modern Doctor. 2021; 59: 6. (In Chinese)

[11] Aliyu M, Zohora FT, Anka AU, Ali K, Maleknia S, Saffarioun M, *et al*. Interleukin-6 cytokine: An overview of the immune regulation, immune dysregulation, and therapeutic approach. International Immunopharmacology. 2022; 111: 109130. https://doi.org/10.1016/j.intimp.2022.109130.

[12] Costa-Pereira AP. Regulation of IL-6-type cytokine responses by MAPKs. Biochemical Society Transactions. 2014; 42: 59–62. https://doi.org/10.1042/BST20130267.

[13] Guo P, Hu Q, Wang J, Hai L, Nie X, Zhao Q. Butorphanol inhibits angiogenesis and migration of hepatocellular carcinoma and regulates MAPK pathway. The Journal of Antibiotics. 2022; 75: 626–634. https://doi.org/10.1038/s41429-022-00565-z.

[14] Meng Z, Li Z, Guo S, Wu D, Wei R, Liu J, *et al*. MED1 Ablation Promotes Oral Mucosal Wound Healing via JNK Signaling Pathway. International Journal of Molecular Sciences. 2022; 23: 13414. https://doi.org/10.3390/ijms232113414.

[15] Manigat LC, Granade ME, Taori S, Miller CA, Vass LR, Zhong XP, *et al*. Loss of Diacylglycerol Kinase α Enhances Macrophage Responsiveness. Frontiers in Immunology. 2021; 12: 722469. https://doi.org/10.3389/fimmu.2021.722469.

[16] Grønhøj MH, Clausen BH, Fenger CD, Lambertsen KL, Finsen B. Beneficial potential of intravenously administered IL-6 in improving outcome after murine experimental stroke. Brain, Behavior, and Immunity. 2017; 65: 296–311. https://doi.org/10.1016/j.bbi.2017.05.019.

[17] Yin N, Wu C, Qiu J, Zhang Y, Bo L, Xu Y, *et al*. Protective properties of heme oxygenase-1 expressed in umbilical cord mesenchymal stem cells help restore the ovarian function of premature ovarian failure mice through activating the JNK/Bcl-2 signal pathway-regulated autophagy and upregulating the circulating of $CD8^{+}CD28^{-}$ T cells. Stem Cell Research & Therapy. 2020; 11: 49. https://doi.org/10.1186/s13287-019-1537-x.

[18] Amini-Nik S, Yousuf Y, Jeschke MG. Scar management in burn injuries using drug delivery and molecular signaling: Current treatments and future directions. Advanced Drug Delivery Reviews. 2018; 123: 135–154. https://doi.org/10.1016/j.addr.2017.07.017.

[19] Soliman AM, Barreda DR. Acute Inflammation in Tissue Healing. International Journal of Molecular Sciences. 2022; 24: 641. https://doi.org/10.3390/ijms24010641.

[20] Wang J, Zhao B, Sun L, Jiang L, Li Q, Jin P. Smart thermosensitive poloxamer hydrogels loaded with Nr-CWs for the treatment of diabetic wounds. PloS One. 2022; 17: e0279727. https://doi.org/10.1371/journal.pone.0279727.

[21] Xie F, Teng L, Lu J, Xu J, Zhang C, Yang L, *et al*. Interleukin-10-Modified Adipose-Derived Mesenchymal Stem Cells Prevent Hypertrophic Scar Formation via Regulating the Biological Characteristics of Fibroblasts and Inflammation. Mediators of Inflammation. 2022; 2022: 6368311. https://doi.org/10.1155/2022/6368311.

[22] Mamilos A, Winter L, Schmitt VH, Barsch F, Grevenstein D, Wagner W, *et al*. Macrophages: From Simple Phagocyte to an Integrative Regulatory Cell for Inflammation and Tissue Regeneration-A Review of the Literature. Cells. 2023; 12: 276. https://doi.org/10.3390/cells12020276.

[23] Cardoso-Lezama I, Ramos-Tovar E, Arellanes-Robledo J, Vargas-Pozada EE, Vásquez-Garzón VR, Villa-Treviño S, *et al*. Serum α-SMA is a potential noninvasive biomarker of liver fibrosis. Toxicology Mechanisms and Methods. 2024; 34: 13–19. https://doi.org/10.1080/15376516.2023.2244061.

[24] Fu D, Yin J, Huang S, Li H, Li Z, Chong T. Rapamycin Inhibits the Growth and Collagen Production of Fibroblasts Derived from Human Urethral Scar Tissue. BioMed Research International. 2018; 2018: 7851327. https://doi.org/10.1155/2018/7851327.

[25] Ge Y, Luo J, Li D, Li C, Huang J, Yu H, *et al*. Deficiency of vitamin D receptor in keratinocytes augments dermal fibrosis and inflammation in a mouse model of HOCl-induced scleroderma. Biochemical and Biophysical Research Communications. 2022; 591: 1–6. https://doi.org/10.1016/j.bbrc.2021.12.085.

[26] Fei H, Qian Y, Pan T, Wei Y, Hu Y. Curcumin alleviates hypertrophic scarring by inhibiting fibroblast activation and regulating tissue inflammation. Journal of Cosmetic Dermatology. 2024; 23: 227–235. https://doi.org/10.1111/jocd.15905.

[27] Cui HS, Lee YR, Ro YM, Joo SY, Cho YS, Kim JB, *et al*. Knockdown of CPEB1 and CPEB4 Inhibits Scar Formation via Modulation of TAK1 and SMAD Signaling. Annals of Dermatology. 2023; 35: 293–302. https://doi.org/10.5021/ad.22.210.

[28] He T, Bai X, Yang L, Fan L, Li Y, Su L, *et al*. Loureirin B Inhibits Hypertrophic Scar Formation via Inhibition of the TGF-β1-ERK/JNK Pathway. Cellular Physiology and Biochemistry: International Journal of Experimental Cellular Physiology, Biochemistry, and Pharmacology. 2015; 37: 666–676. https://doi.org/10.1159/000430385.

[29] Wang Y, Chen Y, Wu J, Shi X. BMP1 Promotes Keloid by Inducing Fibroblast Inflammation and Fibrogenesis. Journal of Cellular Biochemistry. 2024; 125: e30609. https://doi.org/10.1002/jcb.30609.

[30] Qin G, Sun Y, Guo Y, Song Y. PAX5 activates telomerase activity and proliferation in keloid fibroblasts by transcriptional regulation of SND1, thus promoting keloid growth in burn-injured skin. Inflammation Research. 2021; 70: 459–472. https://doi.org/10.1007/s00011-021-01444-3.

[31] Liu L, Song H, Duan H, Chai J, Yang J, Li X, *et al*. TSG-6 secreted by human umbilical cord-MSCs attenuates severe burn-induced excessive inflammation via inhibiting activations of P38 and JNK signaling. Scientific Reports. 2016; 6: 30121. https://doi.org/10.1038/srep30121.

[32] Huang Y, Li S, Chen H, Feng L, Yuan W, Han T. Butorphanol reduces the neuronal inflammatory response and apoptosis via inhibition of p38/JNK/ATF2/p53 signaling. Experimental and Therapeutic Medicine. 2022; 23: 229. https://doi.org/10.3892/etm.2022.11151.

[33] Wong VW, Rustad KC, Akaishi S, Sorkin M, Glotzbach JP, Januszyk M, *et al*. Focal adhesion kinase links mechanical force to skin fibrosis via inflammatory signaling. Nature Medicine. 2011; 18: 148–152. https://doi.org/10.1038/nm.2574.

[34] Ji X, Cui W, Shan S, Liu X, Wang L, Zhang B. Study of ultrasound-guided ropivacaine combined with butorphanol continuous paravertebral block to prevent pain syndrome by evaluating ccl2 gene expression after radical mastectomy. Cellular and Molecular Biology (Noisy-le-Grand, France). 2022; 67: 264–273. https://doi.org/10.14715/cmb/2021.67.4.29.

[35] Yang Z, Wang L, Hu Y, Wang F. Butorphanol protects PC12 cells against OGD/R-induced inflammation and apoptosis. Molecular Medicine Reports. 2020; 22: 1969–1975. https://doi.org/10.3892/mmr.2020.11290.